Digital Implementation of Full-Order Flux Observers for Induction Motors

Marko Hinkkanen and Jorma Luomi
HELSINKI UNIVERSITY OF TECHNOLOGY
Power Electronics Laboratory
P.O. Box 3000, FIN-02015 HUT, Finland
marko.hinkkanen@hut.fi, jorma.luomi@hut.fi
http://www.hut.fi/Units/PowerElectronics/

Keywords

Variable speed drives, induction motors, field oriented control, flux model.

Abstract

This paper deals with flux estimation for induction motor drives by using a full-order flux observer. A problem of full-order flux observers is their need for computationally demanding discretization methods in order to work stably and accurately at high speeds. An implementation of the full-order flux observer using the stator and rotor fluxes as state variables in the stator reference frame and in the rotor reference frame, respectively, was recently proposed. This paper describes how an observer gain can be included in this structure. It is shown that discretization errors of the proposed implementation are small and that there is more freedom to choose an observer gain, even if the simple forward Euler discretization is used.

1 Introduction

Flux estimators are required in high-performance direct field orientation control of induction motors. A full-order flux observer is a versatile choice for both speed-sensored and speed-sensorless drives. It offers good performance and robustness against parameter sensitivity and measurement noise.

The stator current and the rotor flux are conventionally used as state variables in full-order flux observers [1, 2]. Some authors have chosen the stator and rotor fluxes as state variables [3, 4], which enables introducing the observer even into direct torque control or stator flux oriented control. Various reference frames can be used for the implementation: the stator reference frame; the rotor reference frame; or a field oriented reference frame. Properties of the full-order observer, e.g., its dynamics and parameter sensitivity, are controllable through the observer gain.

A well-known problem of full-order flux observers is that they require sophisticated discretization methods in order to work stably and accurately at high speeds (including the nominal speed) [1], [5]–[7]. High-order discrete models are undesirable since they require plenty of real-time calculation. The simple forward Euler discretization

$$\dot{x}(t) \approx \frac{x(t+T_s) - x(t)}{T_s} \tag{1}$$

where T_s is a sampling period, can be used instead. In this case, the stability has to be guaranteed by placing the observer poles inside the stability region corresponding to the discretization. When using a reasonable sampling period, this requirement is difficult to fulfill without sacrificing the versatility of the full-order observer. In other words, the desired properties of the observer cannot be reached due to this limitation. Another problem of the forward Euler discretization is the degraded accuracy due to discretization errors.

Recently, an implementation of the full-order flux observer using the stator and rotor fluxes as state variables in the stator and rotor reference frames was proposed [8]. This natural combination of two

reference frames gives well-behaving observer poles in the whole speed range even with zero observer gain. Consequently, the implementation is well suited to the forward Euler discretization. This paper describes the inclusion of observer gains in the implementation presented in [8]. If desired, very simple observer gains, e.g., real-valued constants, can be chosen. Furthermore, it is shown that the discretization error of this implementation is considerably smaller than that of the conventional implementation.

2 Induction Motor Model

The parameters of the dynamic Γ-equivalent circuit of an induction motor are the stator resistance R_s, the rotor resistance R_R, the stator transient inductance L'_s, and the magnetizing inductance L_M. The electrical angular speed of the rotor is denoted by ω_m, the angular speed of the reference frame ω_k, the stator current space vector $\underline{i}_s$, and the stator voltage $\underline{u}_s$. When the stator flux $\underline{\psi}_s$ and the rotor flux $\underline{\psi}_R$ are chosen as state variables, the state-space representation of the induction motor becomes

$$\dot{\underline{\mathbf{x}}} = \underbrace{\begin{bmatrix} -\frac{1}{\tau'_s} - j\omega_k & \frac{1}{\tau'_s} \\ \frac{1-\sigma}{\tau'_r} & -\frac{1}{\tau'_r} - j\left(\omega_k - \omega_m\right) \end{bmatrix}}_{\underline{\mathbf{A}}} \underline{\mathbf{x}} + \underbrace{\begin{bmatrix} 1 \\ 0 \end{bmatrix}}_{\mathbf{B}} \underline{u}_s \tag{2a}$$

$$\underline{i}_s = \underbrace{\begin{bmatrix} \frac{1}{L'_s} & -\frac{1}{L'_s} \end{bmatrix}}_{\mathbf{C}} \underline{\mathbf{x}} \tag{2b}$$

where the state vector is $\underline{\mathbf{x}} = [\underline{\psi}_s \quad \underline{\psi}_R]^T$, and the parameters expressed in terms of the Γ-equivalent circuit parameters are $\sigma = L'_s/(L_M + L'_s)$, $\tau'_s = L'_s/R_s$, and $\tau'_r = \sigma L_M/R_R$. The block diagram corresponding to (2a) is shown in Fig. 1(a).

3 Full-Order Flux Observer

3.1 Conventional Implementation

The full-order flux observer using the fluxes as state variables is defined by

$$\dot{\hat{\underline{\mathbf{x}}}} = \underline{\mathbf{A}}\,\hat{\underline{\mathbf{x}}} + \mathbf{B}\underline{u}_s + \underline{\mathbf{L}}(\underline{i}_s - \hat{\underline{i}}_s) \tag{3a}$$

$$\hat{\underline{i}}_s = \mathbf{C}\hat{\underline{\mathbf{x}}} \tag{3b}$$

where the observer state vector is $\hat{\underline{\mathbf{x}}} = [\hat{\underline{\psi}}_s \quad \hat{\underline{\psi}}_R]^T$ and the observer gain $\underline{\mathbf{L}} = [\underline{l}_s \quad \underline{l}_r]^T$. Both the stator and rotor electrical dynamics are calculated alternatively in the stator reference frame ($\omega_k = 0$), in the rotor reference frame ($\omega_k = \omega_m$), or in the flux reference frame (where ω_k is the angular speed of the estimated flux). All the implementations based on one reference frame are here called "conventional" even though the stator reference frame is the most usual choice.

Eigenvalues $\underline{\lambda}_{1,2}$ of the observer (3) are obtained by solving the equation

$$\det\left(\underline{\lambda}\mathbf{I} - \underline{\mathbf{A}} + \underline{\mathbf{L}}\mathbf{C}\right) = 0 \tag{4}$$

where $\mathbf{I}$ is a 2×2 identity matrix. The eigenvalue analysis is relevant only if ω_m and ω_k are assumed to be constant. Regardless of the reference frame chosen, there is a speed dependent cross-coupling between the real and imaginary components of at least one state variable. This may lead to poorly damped observer dynamics at high speeds. It is to be noted that the eigenvalues are independent of the choice of state variables.

3.2 Proposed Implementation

In the following, the variables in the stator reference frame are denoted by superscript s and those in the rotor reference frame by superscript m. The state-space representation (2) rewritten using both the stator

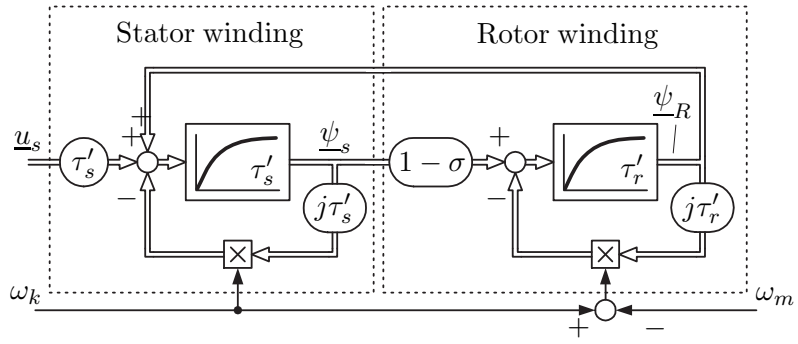

(a)

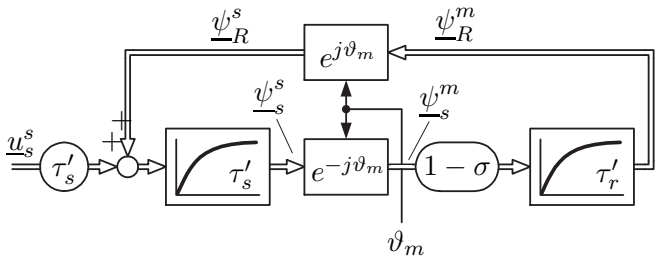

(b)

Figure 1: Block diagram of motor windings (a) in a general reference frame, (b) in the stator (superscript s) and rotor (superscript m) reference frames. Fluxes are used as state variables.

and rotor reference frames is

$$\dot{\underline{\mathbf{z}}} = \underbrace{\begin{bmatrix} -\frac{1}{\tau'_s} & \frac{1}{\tau'_s}e^{j\vartheta_m} \\ \frac{1-\sigma}{\tau'_r}e^{-j\vartheta_m} & -\frac{1}{\tau'_r} \end{bmatrix}}_{\underline{\mathbf{A}}_z} \underline{\mathbf{z}} + \underbrace{\begin{bmatrix} 1 \\ 0 \end{bmatrix}}_{\mathbf{B}} \underline{u}^s_s \tag{5a}$$

$$\underline{i}^s_s = \underbrace{\begin{bmatrix} \frac{1}{L'_s} & -\frac{1}{L'_s}e^{j\vartheta_m} \end{bmatrix}}_{\underline{\mathbf{C}}_z} \underline{\mathbf{z}} \tag{5b}$$

where the state vector is $\underline{\mathbf{z}} = [\underline{\psi}^s_s \quad \underline{\psi}^m_R]^T$ and the angle of rotor ϑ_m. The block diagram corresponding to (5a) is shown in Fig. 1(b). Based on (5), it is natural to form the nonlinear observer[1]

$$\dot{\hat{\underline{\mathbf{z}}}} = \underline{\mathbf{A}}_z\hat{\underline{\mathbf{z}}} + \mathbf{B}\underline{u}^s_s + \underline{\mathbf{L}}_z\big(\underline{i}^s_s - \hat{\underline{i}}^s_s\big) \tag{6a}$$

$$\hat{\underline{i}}^s_s = \underline{\mathbf{C}}_z\hat{\underline{\mathbf{z}}} \tag{6b}$$

where $\underline{\mathbf{L}}_z = \big[\underline{l}_s \quad \underline{l}_r e^{-j\vartheta_m}\big]^T$. The angle of rotor ϑ_m can be directly measured or it can be obtained by integrating the rotor speed ω_m.

If an incremental encoder is used for measuring the rotor speed ω_m, some low-pass filtering of the speed is usually needed. The delay due to this filtering may cause dynamic errors during fast accelerations if the conventional observer implementation is used. In the proposed implementation, the speed ω_m is not needed and the corresponding dynamic errors during fast accelerations are thus avoided.

Eigenvalues Using Floquet Decomposition

For analysis purposes, the observer (6) can be linearized by assuming the angular speed ω_m of the rotor to be constant, leading to a linear time-periodic (LTP) system

$$\dot{\hat{\underline{\mathbf{z}}}} = \underline{\mathbf{A}}_z(t)\hat{\underline{\mathbf{z}}} + \mathbf{B}\underline{u}^s_s + \underline{\mathbf{L}}_z(t)\big(\underline{i}^s_s - \hat{\underline{i}}^s_s\big) \tag{7a}$$

$$\hat{\underline{i}}^s_s = \underline{\mathbf{C}}_z(t)\hat{\underline{\mathbf{z}}} \tag{7b}$$

[1] A similar idea has been preferred in the implementation of reduced-order observers: the voltage model is implemented in the stator reference frame, and the current model in the rotor reference frame [9, Fig. 20].

where the periodic matrices are

$$\underline{\mathbf{A}}_z(t) = \begin{bmatrix} -\frac{1}{\tau_s'} & \frac{1}{\tau_s'}e^{j\omega_m t} \\ \frac{1-\sigma}{\tau_r'}e^{-j\omega_m t} & -\frac{1}{\tau_r'} \end{bmatrix}, \quad \underline{\mathbf{L}}_z(t) = \begin{bmatrix} \underline{l}_s \\ \underline{l}_r e^{-j\omega_m t} \end{bmatrix}, \quad \underline{\mathbf{C}}_z(t) = \begin{bmatrix} \frac{1}{L_s'} & -\frac{1}{L_s'}e^{j\omega_m t} \end{bmatrix} \tag{7c}$$

and the period is $T = 2\pi/\omega_m$. The eigenvalues (or the Lyapunov exponents) of LTP systems can be determined by using the Floquet decomposition [10]. Without loss of generality, the autonomous open-loop system $\dot{\underline{\mathbf{z}}}(t) = \underline{\mathbf{A}}_z(t)\underline{\mathbf{z}}(t)$ with the initial condition $\underline{\mathbf{z}}(t_0) = \underline{\mathbf{z}}_0$ is considered.[2] The solution of the system is $\underline{\mathbf{z}}(t) = \underline{\mathbf{\Phi}}_z(t, t_0)\underline{\mathbf{z}}_0$, where the state transition matrix $\underline{\mathbf{\Phi}}_z(t, \tau)$ satisfies

$$\frac{\partial}{\partial t}\underline{\mathbf{\Phi}}_z(t, \tau) = \underline{\mathbf{A}}_z(t)\underline{\mathbf{\Phi}}_z(t, \tau), \quad \underline{\mathbf{\Phi}}_z(\tau, \tau) = \mathbf{I} \tag{8}$$

For a linear T-periodic system, the state transition matrix $\underline{\mathbf{\Phi}}_z(t+T, t)$ is a periodic matrix and its eigenvalues are independent of t. A constant system matrix $\tilde{\underline{\mathbf{A}}}_z$ corresponding to the periodic matrix $\underline{\mathbf{A}}_z(t)$ can be obtained based on the Floquet decomposition by solving $e^{\tilde{\underline{\mathbf{A}}}_z T} = \underline{\mathbf{\Phi}}_z(T, 0)$. The eigenvalues of $\tilde{\underline{\mathbf{A}}}_z$ are the Lyapunov exponents of the system. In practice, the state transition matrix $\underline{\mathbf{\Phi}}_z(T, 0)$ can be evaluated by using time-domain simulation of (8).

Eigenvalues Using Coordinate Transformation

Another, simpler method is to transform the eigenvalues of the conventional observer implementation (3) to the stator and rotor reference frames. The eigenvalue of (3) corresponding to the rotor dynamics calculated in the stator reference frame is transformed to the rotor reference frame using [11]

$$\underline{\lambda}_2^m(\omega_m) = \mathrm{Re}\left\{\underline{\lambda}_2^s(\omega_m)\right\} + j\,\mathrm{Im}\left\{\underline{\lambda}_2^s(\omega_m)\right\} + j\omega_m \tag{9}$$

The eigenvalue corresponding to the stator dynamics, $\underline{\lambda}_1^s$, is not transformed. Both the Floquet decomposition approach and the coordinate transformation approach give the same result.

3.3 Comparison of Discretization Errors of System Matrices

Two major factors affecting the accuracy of the estimated states are the discretization errors of the elements of the discretized system matrix and the frequencies of the estimated states. In the following, the errors of the system matrix are studied, and the effect of the frequencies are then discussed.

The open-loop system matrix (i.e., $\underline{l}_s = \underline{l}_r = 0$) is first considered. The accurately discretized system matrix of the conventional implementation corresponds to the state transition matrix

$$\underline{\mathbf{\Phi}}(T_s, 0) = \exp(T_s\underline{\mathbf{A}}) = \mathbf{I} + \frac{T_s\underline{\mathbf{A}}}{1!} + \frac{T_s^2\underline{\mathbf{A}}^2}{2!} + \ldots \tag{10}$$

The state transition matrix of the proposed implementation $\underline{\mathbf{\Phi}}_z(T_s, 0)$ can be calculated by using (8). The system matrices discretized using the forward Euler method are $\underline{\mathbf{A}}_d = \mathbf{I} + T_s\underline{\mathbf{A}}$ and $\underline{\mathbf{A}}_{zd} = \mathbf{I} + T_s\underline{\mathbf{A}}_z$ for the conventional and proposed implementations, respectively.

In Fig. 2, the normalized discretization errors of the open-loop system matrices of the conventional implementation in the stator reference frame and the proposed implementation are depicted when the forward Euler discretization is used. The parameters of a 2.2-kW four-pole induction motor given in Table I were used. It can be seen that the discretization errors at high speeds can be considerably reduced by using the proposed implementation. In the conventional method, the rotor reference frame or the flux reference frame could be used instead of the stator reference frame. The change of the reference frame has only a marginal influence on the errors of system matrices in Fig. 2.

In the proposed implementation, the steady-state frequency of the stator flux estimate corresponds to the stator frequency whereas the steady-state frequency of the rotor flux estimate corresponds to the slip frequency. In the conventional implementation, the steady-state frequencies of both the flux estimates are equal. The frequency depends on the chosen reference frame: the stator, rotor, and flux reference frames correspond to the stator, slip, and zero frequencies, respectively.

[2] Firstly, the input $\mathbf{B}\underline{u}_s^s$ does not affect to the eigenvalues and, secondly, the closed-loop system can be easily arranged to this form by replacing $\underline{\mathbf{A}}_z$ with $\underline{\mathbf{A}}_z - \underline{\mathbf{L}}_z\underline{\mathbf{C}}_z$.

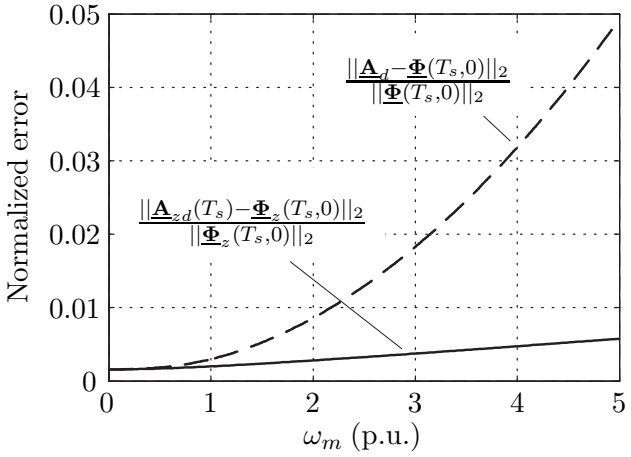

Figure 2: Comparison of normalized discretization errors of the open-loop system matrices when the forward Euler discretization is used. The dashed line shows the error corresponding to the conventional implementation ($\omega_k = 0$) and the solid line the error corresponding to the proposed implementation.

Table I: Parameters for the 2.2-kW four-pole 400-V 50-Hz motor.

Stator resistance R_s	3.67 Ω
Rotor resistance R_R	2.10 Ω
Magnetizing inductance L_M	0.224 H
Stator transient inductance L'_s	0.0209 H
Moment of inertia J_{tot}	0.0155 kgm^2
Rated speed	1430 r/min
Rated current	5.0 A
Rated torque	14.6 Nm

Due to the signal frequency being zero in the steady state, the actual errors of the estimated states are slightly smaller if the conventional method in the synchronous reference frame is used. However, the poor damping of the observer dynamics is still present in the conventional implementation. In the proposed implementation, the damping is much better and more freedom to choose the observer gain is left.

3.4 Parameter Sensitivity

The effect of motor parameter deviations can be analyzed by the means of steady-state relations [9, 12]. It is easy to show that the parameter sensitivity analysis is equivalent for both the conventional and proposed implementations when the same $\underline{l}_s$ and $\underline{l}_r$ are used.

4 Observer Gains

The eigenvalues of the observer resulting from three gain selections are shortly analyzed using the parameters of the 2.2-kW four-pole induction motor. The gains are chosen to illustrate the general differences between the conventional and proposed implementations. Furthermore, they are chosen to be usable also in the speed-sensorless case when the observer is augmented by a speed-adaptation loop, e.g., [4]. It is, however, to be noted that the speed-adaptation loop has an influence on the eigenvalues of the observer.

In order to get a stable forward Euler discretization using the sampling period T_s, the poles of the continuous time system should be located inside a circle with radius $1/T_s$ centered at $\{-1/T_s, 0\}$. This stability region is plotted (dashed line) in the following root loci plots assuming a sampling period of 200 μs.

4.1 Open-Loop Eigenvalues

The open-loop eigenvalues are obtained by choosing $\underline{l}_s = \underline{l}_r = 0$. In Fig. 3(a), the root loci of the conventional implementation (3) in the rotor reference frame are plotted when the rotor speed ω_m varies from 0 to 5 p.u. As the speed ω_m increases, the magnitude of the imaginary part of the eigenvalue corresponding to the rotor dynamics increases. This leads to instability at higher speeds (in this case at

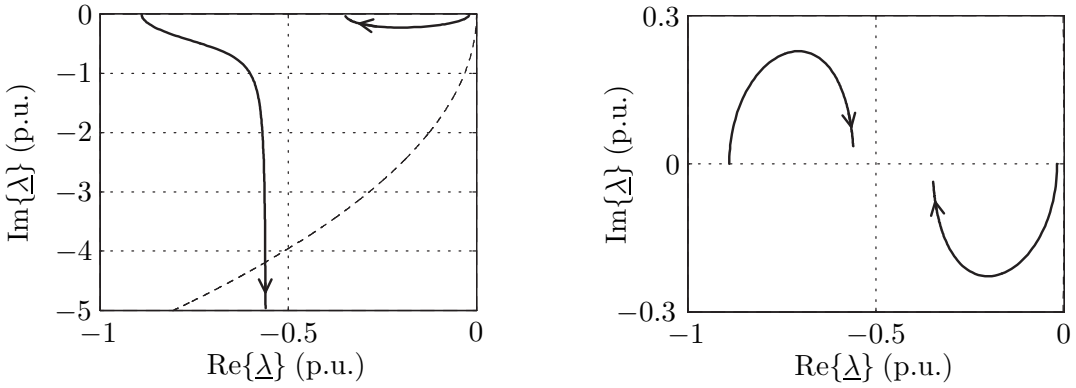

Figure 3: Observer root loci plotted, when $\omega_m = 0 \ldots 5$ p.u., $\underline{l}_s = \underline{l}_r = 0$. (a) the conventional implementation in the rotor reference frame, and (b) the proposed implementation.

speeds higher than approximately 4.2 p.u.) if the forward Euler discretization is used. Fig. 3(b) shows the root loci of the proposed implementation (6). The eigenvalues behave well in the whole speed range.

The root loci of Fig. 3(a) correspond to the loci plotted in the flux reference frame with the slip angular frequency ω_r being zero. Nonzero slip would just slightly shift the loci vertically, i.e., $-j\omega_r$ is added to the eigenvalues calculated in the rotor reference frame. When the stator reference frame is used, the instability occurs at much lower speeds. In the case of larger machines, the instability is faced at lower speeds since the real parts of the eigenvalues of larger machines are smaller.

4.2 Shifted Open-Loop Eigenvalues

In order to have faster convergence of the estimation error, the open-loop eigenvalues can be shifted to the left in the complex plane. The eigenvalues of the observer are explicitly determined as $-k(\frac{1}{\tau'_s}+\frac{1}{\tau'_r})+\underline{\lambda}_{1,2}$, where $\underline{\lambda}_{1,2}$ are the open-loop eigenvalues of the induction motor and k is a shifting factor [4]. This pole placement leads to the complex-valued speed-varying observer gain

$$\underline{l}_s = \frac{kL'_s}{\tau'_s}\frac{\tau'_s+\tau'_r}{(\omega_m\tau'_r)^2+\sigma^2}\left[\frac{(k+1)\sigma(\tau'_s+\tau'_r)}{\tau'_s\tau'_r} + \omega_m^2\tau'_r + j\omega_m\left(\frac{(k+1)(\tau'_s+\tau'_r)}{\tau'_s} - \sigma\right)\right] \tag{11a}$$

$$\underline{l}_r = \frac{kL'_s}{\tau'_s}\frac{\tau'_s+\tau'_r}{(\omega_m\tau'_r)^2+\sigma^2}\left[\frac{(k+1)\sigma(\tau'_s+\tau'_r)}{\tau'_s\tau'_r} - \omega_m^2\tau'_r - \frac{2\sigma^2}{\tau'_r} + j\omega_m\left(\frac{(k+1)(\tau'_s+\tau'_r)}{\tau'_s} - \sigma\right)\right] \tag{11b}$$

The root loci correspond to the loci shown in Fig. 3 besides that they are shifted to the left. The weakness of the shifted open-loop eigenvalues in the speed-sensored case is high sensitivity to parameter inaccuracies unless k is small (for the given 2.2-kW motor, $k > 0.2$ leads to high sensitivity). A benefit is that higher speeds can be reached compared with the zero-gain case (in the case of the conventional implementation).

4.3 Constant Gain

A simple observer gain is obtained by choosing constant $\underline{l}_s$ and $\underline{l}_r$. Despite the simplicity of this observer gain, good parameter sensitivity properties in the motoring region can be obtained if the constant gain is suitably chosen [3]. For the given motor, $\underline{l}_s = 5R_s$ and $\underline{l}_r = 0$ were chosen. The root loci of the conventional implementation in the stator reference frame and the proposed one are shown in Figs. 4(a) and 4(b), respectively. The conventional implementation using the forward Euler discretization is unstable at speeds higher than approximately 1.8 p.u. whereas the proposed implementation is stable.

An interesting special case is obtained by choosing $\underline{l}_r = R_R$. The proposed implementation of the full-order observer then reduces to the well-known current model implemented in the rotor reference frame.

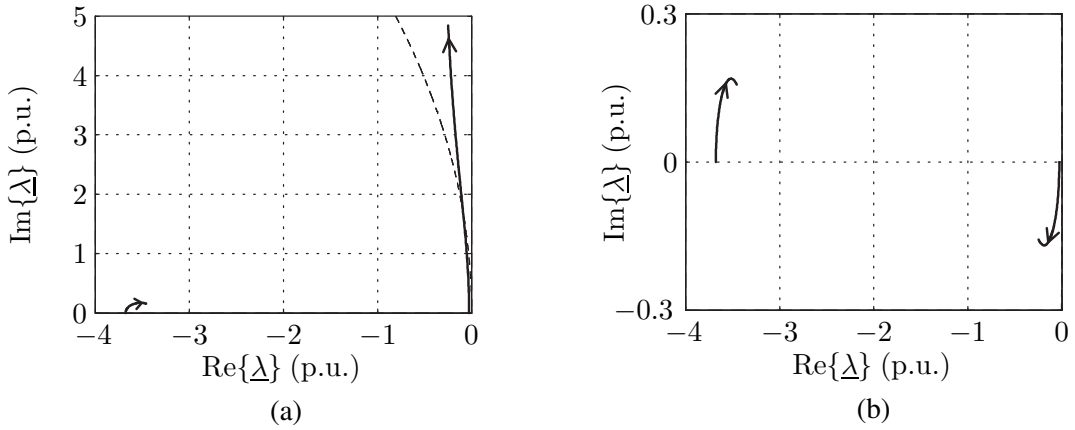

Figure 4: Observer root loci plotted, when $\omega_m = 0 \ldots 5$ p.u., $\underline{l}_s = 5R_s$, $\underline{l}_r = 0$. (a) the conventional implementation in the stator reference frame, and (b) the proposed implementation.

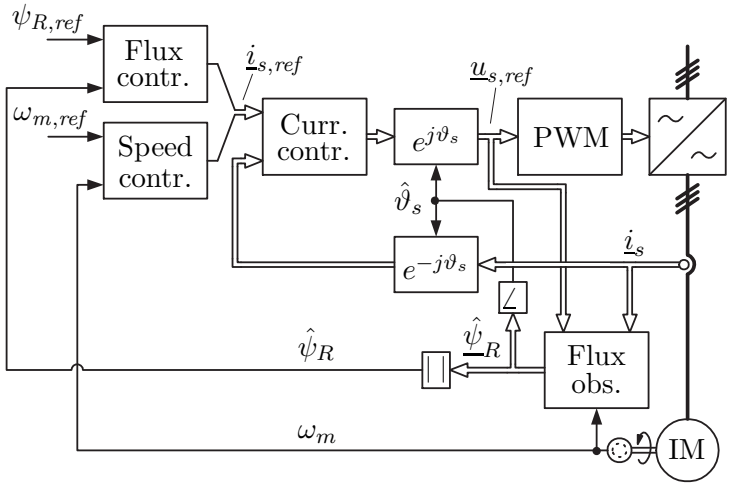

Figure 5: The direct rotor flux oriented controller. The electrical variables shown on the left-hand side of the coordinate transformations are in the (estimated) rotor flux reference frame and the variables on the right-hand side are in the stator reference frame.

5 Control System

The proposed and conventional observer implementations were also investigated experimentally. The control was based on the direct rotor flux orientation and synchronous-frame current control [13, 14]. The simplified overall block diagram of the system is shown in Fig. 5.

The speed and flux controllers were conventional PI-controllers. The bandwidths of the controllers are given in Table II. The sampling was synchronized to the modulation, and both the switching frequency and the sampling frequency were 5 kHz. The dc-link voltage was measured, and the reference stator voltage obtained from the current controller was used for the flux observer.

6 Experimental Results

The experimental setup consists of the 2.2-kW four-pole induction motor which is fed by a frequency converter controlled by a dSpace DS1103 PPC/DSP board. The base values used in the figures are: angular frequency $2\pi \cdot 50$ s^{-1}, current $\sqrt{2} \cdot 5.0$ A, and flux 1.0 Wb.

In the first experiment, the zero observer gain was chosen. An experiment using the conventional implementation in the rotor flux reference frame is shown in Fig. 6(a), and an experiment using the proposed implementation is shown in Fig. 6(b). The speed reference was stepped from zero to 5 p.u. at $t = 0.5$ s. No external load torque was applied. The drive was operating in the overmodulation region even in the steady state due to high mechanical losses at high speeds. As expected based on the root loci of Fig. 3, the conventional implementation turned into instability whereas the proposed implementation remained stable.

Table II: Bandwidths, base value $2\pi \cdot 50\ \mathrm{s}^{-1}$.

Current control	$\alpha_c = 8$ p.u.
Speed control	$\alpha_s = 0.05\alpha_c$
Flux control	$\alpha_f = \alpha_s$

In the second experiment, the observer gain was chosen to be $\underline{l}_s = 5R_s, \underline{l}_r = 0$ corresponding to that used in the root loci of Fig. 4. Figs. 7(a) and 7(b) show experimental results obtained using the conventional implementation in the stator reference frame and the proposed implementation, respectively. The speed reference was stepped from zero to 1.8 p.u. at $t = 0.2$ s. Correspondence between the root loci and the experiments is again very good; the conventional implementation became unstable whereas the proposed one remained stable. The subharmonic frequency (equal to ω_m/p) seen in the torque producing current component i_{sq} originates from the speed measurement.

It is to be noted that the bandwidth of the flux controller was high. Therefore, the flux estimate tries to follow its reference, and the instability or inaccuracies of the flux estimation (due to discretization errors or inaccurate motor parameters) can be seen in the flux producing current component i_{sd}. In the base-speed region, the current i_{sd} should be ideally constant. However, it can be seen that i_{sd} in Fig. 7(a) reduces significantly in the base-speed region ($t = 0.2 \ldots 0.3$ s) along with the increasing speed. This is due to discretization errors of the conventional observer implementation.

In Figs. 6(a) and 6(b), the current component i_{sd} varies moderately in the base-speed region whereas in Fig. 7(b) it remains almost constant. This difference is probably due to the zero-observer-gain case being more sensitive to inaccuracies in the motor parameters used.

7 Conclusions

The proposed observer implementation has several advantages as compared with conventional implementations: (a) well-behaving observer poles are obtained in the whole speed range even without observer gain; (b) discretization errors are small even if the simple forward Euler discretization is used; (c) there is more freedom to choose the observer gain if the forward Euler discretization is used; and (d) dynamic errors due to the possible filtering of the measured rotor speed are eliminated. Furthermore, the observer gain can be selected by using conventional methods, and the results of the parameter sensitivity analysis for the conventional observer implementation can be used. The observer can also be augmented with existing parameter (or speed) adaptation rules.

References

[1] G. Verghese and S. Sanders, "Observers for flux estimation in induction machines," *IEEE Transactions on Industrial Electronics*, vol. 35, pp. 85–94, Feb. 1988.

[2] H. Kubota, K. Matsuse, and T. Nakano, "DSP-based speed adaptive flux observer of induction motor," *IEEE Transactions on Industry Applications*, vol. 29, pp. 344–348, Mar./Apr. 1993.

[3] B. Peterson, *Induction machine speed estimation – observations on observers*. PhD thesis, Department of Industrial Electrical Engineering and Automation, Lund University, Lund, Sweden, Feb. 1996.

[4] J. Maes and J. Melkebeek, "Speed-sensorless direct torque control of induction motors using an adaptive flux observer," *IEEE Transactions on Industry Applications*, vol. 36, pp. 778–785, May/June 2000.

[5] O. Vainio, S. Ovaska, and J. Pasanen, "A digital signal processing approach to real-time AC motor modeling," *IEEE Transactions on Industrial Electronics*, vol. 39, pp. 36–45, Feb. 1992.

[6] C. Bottura, J. Silvino, and P. de Resende, "A flux observer for induction machines based on a time-variant discrete model," *IEEE Transactions on Industry Applications*, vol. 29, pp. 349–354, Mar./Apr. 1993.

[7] G. Griva, P. Ferraris, F. Profumo, R. Bojoi, R. Maceratini, and G. Barba, "Luenberger observer for high speed induction machine drives based on a new pole placement method," in *9th European Conference on Power Electronics and Applications (EPE'01)*, (Graz, Austria), Aug. 2001.

[8] M. Hinkkanen and J. Luomi, "Novel full-order flux observer structure for speed sensorless induction motors," in *The 27th Annual Conference of the IEEE Industrial Electronics Society (IECON'01)*, vol. 2, (Denver, CO), pp. 1333–1338, Nov./Dec. 2001.

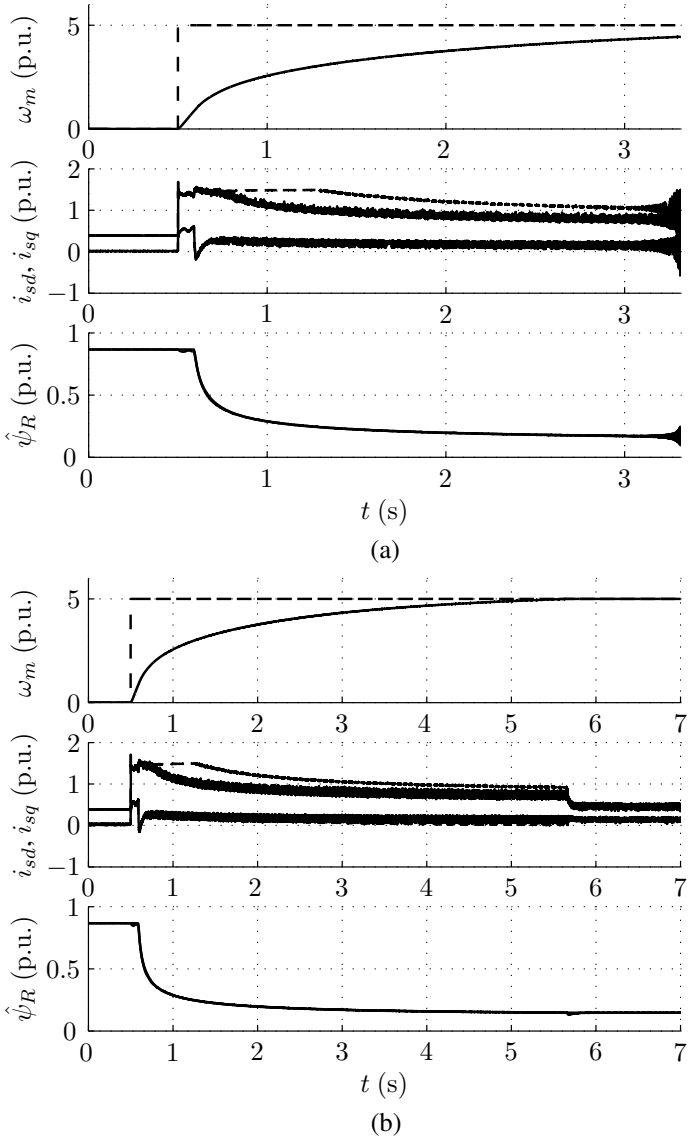

Figure 6: Experimental results obtained using (a) the conventional implementation in the rotor flux reference frame and (b) the proposed implementation. The observer gain is $\underline{l}_s = \underline{l}_r = 0$ corresponding to the root loci in Fig. 3. The first subplot shows the measured speed (solid) and the speed reference (dashed). The second subplot shows the measured d and q components of the stator current (solid) and their references (dashed) in the estimated rotor flux reference frame. The third subplot presents the magnitude of the estimated rotor flux (solid) and its reference (dashed).

[9] P. Jansen and R. Lorenz, "A physically insightful approach to the design and accuracy assessment of flux observers for field oriented induction machine drives," *IEEE Transactions on Industry Applications*, vol. 30, pp. 101–110, Jan./Feb. 1994.

[10] W. Rugh, *Linear System Theory*. Upper Saddle River, NJ: Prentice-Hall, 2nd ed., 1996.

[11] J. Holtz, "On the spatial propagation of transient magnetic fields in AC machines," *IEEE Transactions on Industry Applications*, vol. 32, pp. 927–937, July/Aug. 1996.

[12] M. Hinkkanen and J. Luomi, "Parameter sensitivity of full-order flux observers for induction motors," in *Conference Record of the IEEE Industry Applications Conference, Thirty-Seventh IAS Annual Meeting*, (Pittsburgh, PA), Oct. 2002. In press.

[13] L. Harnefors and H.-P. Nee, "Model-based current control of AC machines using the internal model control method," *IEEE Transactions on Industry Applications*, vol. 34, pp. 133–141, Jan./Feb. 1998.

[14] F. Briz, M. Degner, and R. Lorenz, "Analysis and design of current regulators using complex vectors," *IEEE Transactions on Industry Applications*, vol. 36, pp. 817–825, May/June 2000.

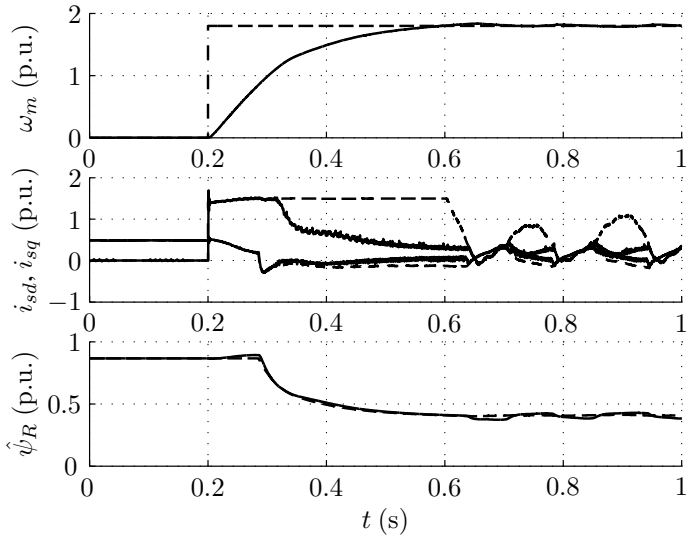

(a)

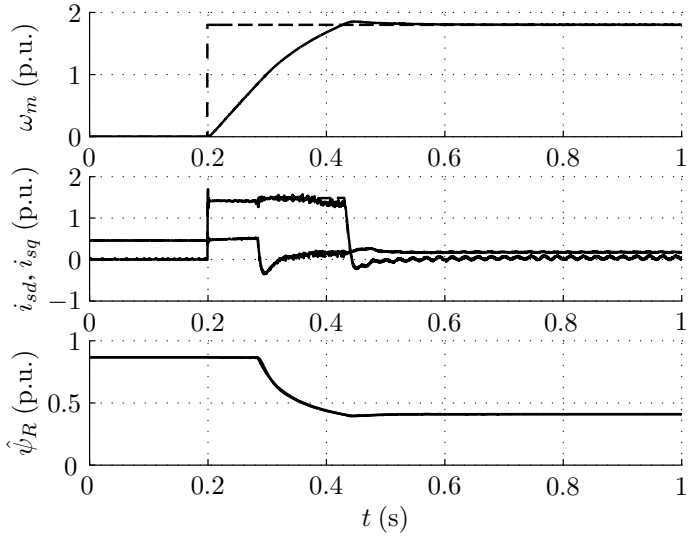

(b)

Figure 7: Experimental results obtained using (a) the conventional implementation in the stator reference frame and (b) the proposed implementation. The observer gain is $\underline{l}_s = 5R_s$, $\underline{l}_r = 0$, corresponding to the root loci in Fig. 4. Explanations of the curves are given in Fig. 6.